npj | climate and atmospheric science

www.nature.com/npjclimatsci

ARTICLE OPEN

Check for updates

Possible factors for the recent changes in frequency of central Indian Summer Monsoon precipitation extremes during 2005–2020

C. Bajrang[1], Raju Attada[1]✉ and B. N. Goswami[2]

The transitions of short-term trends of Indian Summer Monsoon daily precipitation extremes remain poorly understood. Here, we show a short-term declination of temporal frequency of monsoonal precipitation extremes over Central India for the last 15 years starting from 2005 to 2020 while the low and moderate events show increasing trends. The possible dynamical and thermodynamical factors for the observed decline in precipitation extremes include depletion in moisture transport to Central India via cross-equatorial flow and the low-level Somali jet, caused by reduced evaporation from the regional moisture sources. In addition, the vertical gradient of the moist static energy exhibits favorable conditions for increased lower atmospheric stability, supporting the declining trends. Lastly, the Atlantic Zonal Mode seems to be a potential large-scale climate driver for the less frequent central Indian extreme rainfall events during 2005–2020.

npj Climate and Atmospheric Science (2023)6:120 ; https://doi.org/10.1038/s41612-023-00450-y

INTRODUCTION

The most dominant modulators of the global climate in the recent era have been the number of anthropogenically induced forcings, causing climate change via global warming and the subsequent alterations of the planetary hydroclimate[1]. Understanding the climate responses through models and predictions faces many difficulties, primary amongst those being the spatial heterogeneity[2]. Nowhere is it more challenging than in the tropics, where past climate models have consistently had issues with matching the observational rainfall data[3], with its active water cycles[4]. The global knowledge of the hydroclimate response has been geared towards the warm-gets-wetter[5,6] or the wet-gets-wetter[7–9] schools of thought in the tropics including the tropical monsoon regions. Although it is expected that climate change will lead to increased precipitation[10–12], the ground reality has been quite different with cases like the Indian Summer Monsoon rainfall (ISMR) exhibiting an extended declining trend of mean precipitation for the period between 1950 and 2002[13,14]. Other studies have shown that ISMR has a significant multi-decadal variability with the period between 60 and 70 years[15–17] and the decreasing trend of ISMR from 1950 is a manifestation of a decreasing phase of the multi-decadal variability. More recent study[18] indicating a revival of ISMR to an increasing trend from 2002 supports such a hypothesis that short-term trends of ISMR are related to the multi-decadal variability.

The Indian Summer Monsoon is a convectively coupled system, the large-scale winds are a result of a response to latent heat source from monsoon rainfall while the convergence of moisture by the same winds sustains and strengthens the rainfall. Therefore, large-scale wind indices of Indian monsoon correlate significantly with the seasonal precipitation[19,20]. However, due to the 'internal' variability of the convectively coupled system, this relationship is not very strong[21,22]. Therefore, the multi-decadal variability of ISMR is expected to also manifest in similar multi-decadal variability in wind indices like the monsoon Hadley index or low-level westerly jet (LLJ) index, etc. Further, as the extreme rainfall events (EREs) are the results of convective instability on the background mean monsoon condition, the multi-decadal variability of ISMR is expected to lead to multi-decadal variability of statistics of EREs over the region. Some studies show that indeed the daily EREs over Central India (CI) as well as over Northeast India (NEI) have multidecadal variability[21–23]. Therefore, the short-term trends of the EREs are largely a part of the multi-decadal variability of the EREs. It has also been suggested that the changes in land-use/land-cover patterns owing to urbanization and other human-induced factors, along with regional thermodynamical, dynamical, and convective parameters, are known to have correlational and causal relationships with the ISM rainfall[24]. Forewarning of the transition of trends of EREs such as from a decreeing to an increasing is of great interest for disaster preparedness planning but a long-range prediction remains challenging due to the 'chaotic' nature of the climate system. Here, we identify such a transition from decreasing trend to an increasing trend of EREs in recent history and investigate the potential drivers for this transition with the hope that findings will help develop a long-lead prediction of statistics of the EREs.

The major precipitation regimes (based on the intensity) at CIR, include Light Rainfall Events ($0 < \text{LREs} \leq 5$ mm/day), Moderate Rainfall Events (5 mm/day $<$ MREs $\leq$ 100 mm/day), High Rainfall Events (100 mm/day $<$ HREs $\leq$ 150 mm/day), and Extreme Rainfall Events (150 mm/day $<$ EREs)[25]. Among these regimes, LREs and MREs are fruitful to the human population as these feed the agriculture in the region, whereas HREs and EREs are often associated with the destruction of properties and livelihoods[26,27]. It may be noted that the precipitation in HREs and EREs comes from smaller sub-mesoscale deep convective systems (sometimes independently but often in the environment of a synoptic scale disturbance) and contributes to about 7% to the seasonal total rainfall while that in LREs and MREs come from convective clusters and synoptic scale low-pressure systems (LPS) and contributes to more than 90% of seasonal rainfall[15]. In this study, we show that

[1]Department of Earth and Environmental Sciences, Indian Institute of Science Education and Research Mohali, Mohali, Punjab 140306, India. [2]Department of Physics, Cotton University, Guwahati, Assam 781001, India. ✉email: rajuattada@iisermohali.ac.in

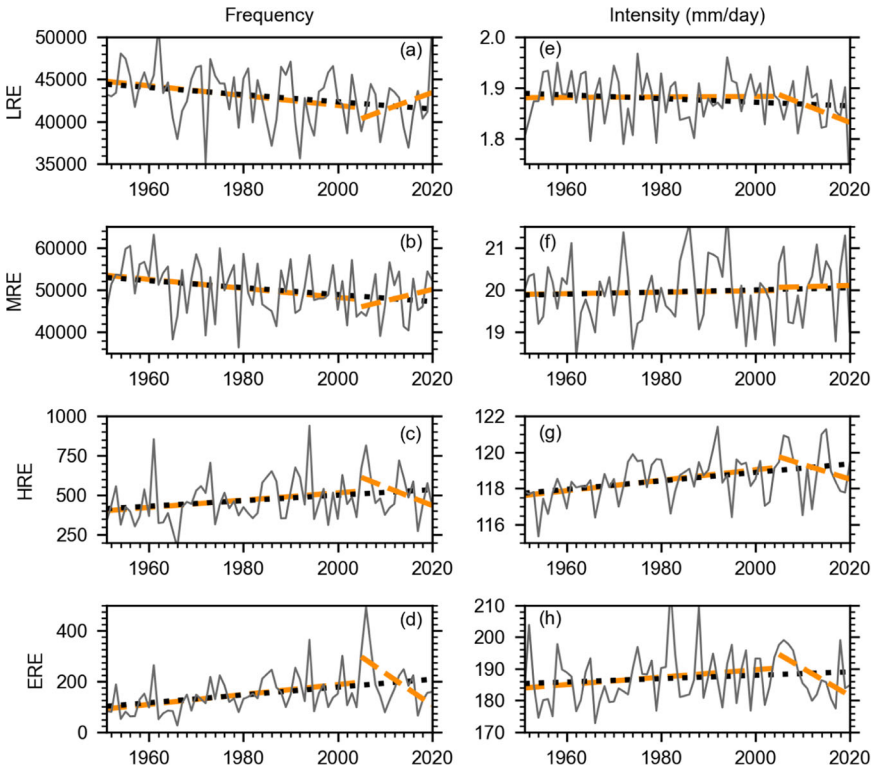

Fig. 1 Trends of precipitation regimes in Central India. Time Series of the frequency (numbers) and intensity (mm/day) of **a**, **e** LREs, **b**, **f** MREs, **c**, **g** HREs, and **d**, **h** EREs, respectively, during ISM in CIR. The dotted black lines indicate the overall linear trends from 1951 to 2020, with the orange dashed lines indicating linear trends from 1951 to 2005 and from 2005 to 2020. Dataset Utilized: IMD 0.25°.

low-level MSE or CAPE during the summer over CIR is conducive for HREs and EREs to occur. When the humidity level exceeds a critical level supported by large-scale background, the instability initiates an intense convective event. The local low pressure converges moisture from a much larger surrounding area (more than five times the radius of the local convective event), further intensifies the event, and creates the HREs and EREs. Thus, HREs and EREs temporarily dry out the larger-scale environment. Through diffusion and advection, an equilibrium is restored but in the intervening period, the LREs and MREs are inhibited. Therefore, the frequency of occurrence of HREs/EREs and LREs/MRE are always complementary with increasing trends of frequency of HREs/EREs being associated with decreasing trends LREs/MRE decrease and vice versa.

In this study, we will focus exclusively on the EREs owing to their sheer socio-economic importance. There have been numerous studies that have been conducted towards studying the trends and the mechanisms of EREs in CIR during ISM[15,23,28]. Most of those studies, which have variously included precipitation data from 1901 to 2020, have found an overall generally significant rising trend in ISM ERE frequency, with the moderate rainfall frequency and the mean precipitation having declining trends[15], agreeing with the pre-existing relations among the regimes[29,30]. Precisely the same conclusions can be reached from the concurrent analysis in Fig. 1, showing declining trends for LREs and MREs and rising trends for HREs and EREs till 2020 since 1951, which agrees with the expected response of precipitation trends to climate change. However, a finer look at the temporal periods is known to have revealed that these patterns are not the same during both the active and break spells of ISM[31]. Even not minding these active and break periods, we have observed that the overall trends increase only during the first 50 or 55 years since 1951, with the trends since the turn of the millennium indicating the exact opposite patterns in frequency throughout all the regimes. The statistical significance of these trends is reported in Table 1. Most significantly, it is observed that the EREs are in a weakening phase for roughly the last two decades, both in rainfall event count and intensity (Fig. 1, Table 2). Such smooth agreement between the frequency and intensity cannot be said for the other regimes, except the HREs. The linear trends of LRE and MRE intensities possess no statistical significance (Table 2).

What is responsible for the declining trend of EREs over CIR during recent years? From Supplementary Fig. 1, it is clear that this decline may be part of a larger 50–70-year multi-decadal oscillation[23,32]. Therefore, even though the long-term ERE trend is an increasing one, the short-term trends are associated with the multi-decadal variability of the EREs. However, due to the aperiodicity of the multidecadal variability, forewarning of transitions from one to the other is formidable. Hence, finding the possible factors as to why and how such a decline could persist and exist in a warming world, other than the orography-induced ERE drops[33], deserves a detailed investigative analysis, which is the foremost aim of this study.

In this undertaking, the study utilizes multiple precipitation datasets with the dominant dataset chosen for analysis being the Indian Meteorological Department's (IMD) long-term daily gridded dataset[34], spanning 1901 to 2020 with a high resolution of 0.25°. This daily gridded rainfall dataset is based on a variable rain gauge network with a total number of stations over the country ranging from about 1500 in 1901 to 6000 in recent years. Also, the daily mean over any region (for example, CIR) is based on different sets of stations reporting rain on different days. As a result, there is potential for artificial variability (or trend) introduced due to the variable station network[35]. However, the trend of EREs from this dataset during 1951–2005 agrees well with that obtained with another daily dataset based on a fixed station network[23]. Therefore, we believe that the 'artificial variability' or trend introduced during the period under consideration 1951–2005 may be minimal. In

Table 1. Precipitation regime-wise frequency trends pre (per 55 years) and post-2005 (per 16 years), between 1951 and 2020, obtained from the Modified Mann–Kendall test.

	Pre-2005			Post-2005		
	Trend	Trend Value	*P*-value	Trend	Trend value	*P*-value
LRE	Dec	−2962.33	2.19667e−10	No	+834.667	0.53293
MRE	Dec	−6336.58	1.43279e−11	Inc	+5265.60	0.01930
HRE	Inc	+120.132	2.51021e−12	Dec	−176.533	0.00054
ERE	Inc	+98.4211	0.0	Dec	−165.067	0.00385

Here, Inc, Dec, & No represent Rising, Declining, and Not Statistically Significant trends, respectively. Dataset Utilized: IMD 0.25°.

Table 2. Precipitation regime-wise intensity trends pre (mm/day/55 years) and post-2005 (mm/day/16 years), between 1951 and 2020, obtained from the Modified Mann–Kendall test.

	Pre-2005			Post-2005		
	Trend	Trend value	*P*-value	Trend	Trend value	*P*-value
LRE	No	−0.00160	0.84807	No	−0.03071	0.47633
MRE	No	+0.02373	0.86787	No	+0.36518	0.40273
HRE	Inc	+1.64490	1.83193e−09	Dec	−1.80410	0.00746
ERE	Inc	+7.70811	1.40266e−08	Dec	−17.4516	0.00261

Here, Inc, Dec, & No represent Rising, Declining, and Not Statistically Significant trends, respectively. Dataset Utilized: IMD 0.25°.

particular, as the total number of stations during the recent two decades is very large (~6000), we have high confidence in the declining trend during the past 15 years. In order to test the robustness of the recent trends of EREs, the IMD dataset is supplemented by two other rainfall datasets from the Tropical Rainfall Measurement Mission (TRMM) 3B42[36] and the Integrated Multi-SatellitE Retrievals for Global Precipitation Measurement (GPM IMERG)[37] respectively, which are both satellite-based daily observational datasets. Both the datasets span from 1998 and 2000 to the present, with the former having a spatial resolution of 0.25° and the latter having an even higher resolution of 0.1°. For the various thermodynamic and dynamic parameters, the European Center for Medium-Range Weather Forecasts Reanalysis 5 (ERA5)[38,39] with a resolution of 0.25° was employed. Whereas, the sea surface temperature is taken from the Extended Reconstructed Sea Surface Temperature (ERSST) V5 dataset[40], available at the 2° × 2° resolution.

The first step in the analysis involves identifying and establishing the problem with certainty. This calls for verifying the robustness of the declining ERE trends over recent years with respect to the datasets and the definitions. For the next part, which moves towards answering how and why this trend persists, we will look into both dynamic and thermodynamic aspects, which includes understanding the role of the regional moisture sources and the local moist thermodynamic parameters. While the dynamics may explain the fixture of the observed trends on the bigger regional and global scales, the thermodynamics may be more geared towards identifying the physical processes that drive the decline on a local scale. With the region of focus being in the tropics, it is also necessary to understand the part of the regional and seasonal Hadley circulation cell and the numerous possible long-term tropical climate drivers in driving the recent declining modulation of CIR ISM EREs.

RESULTS AND DISCUSSION

As mentioned earlier, the increasing trends of the frequency of occurrences of EREs are evident from 1951 to the first decade of the 21st century[15,28]. With global warming and the warming of the Indian sub-continent unabated during the past two decades[41–43], it is counterintuitive to think that the EREs could decrease during this period. However, on top of the long-term increasing trend of the EREs driven by climate change, there could be multi-decadal oscillations[22] and the change of trends at this juncture may be associated with the change of phase of multi-decadal variability of the EREs. That is what seems to have happened during the past two decades as seen from Fig. 1 where we note that the rising trends in EREs do not last for the entirety of the time till the present, ending at approximately the beginning of the millennium. Since the turn of the century, the ERE frequency trend is found to have switched signs, showing a general decline. Through breakpoint analysis and trend-based p-value analysis (Supplementary Table 1), this decline is confirmed to be the most statistically significant in the period between 2005 and 2020. Thus, these years are chosen to be the general time period of decline for the rest of the study. It ought also to be noted that the trend is negative even after omitting the peak in 2006.

The robustness across datasets for these inferences is confirmed in Supplementary Fig. 2, by checking the temporal patterns of ERE frequency since 2005 from TRMM and GPM IMERG, which both agree well with that obtained from the IMD data. It may be noted that the higher resolution GPM IMERG dataset has the most statistically significant trends, as can be seen in Supplementary Table 1.

It has been known from previous studies that the frequency of EREs is sensitive to the definition used in choosing what constitutes an ERE. In order to eliminate the possibility of the ERE definition skewing[44] the observed trends, the spatially variable percentile thresholds are also utilized and tested for robustness. As can be seen from Supplementary Fig. 3, all four chosen percentiles (99th, 99.5th, 99.9th, and 99.99th) agree well with the patterns obtained from the absolute threshold definition, across all the three chosen rainfall datasets. The exclusion of a spatial component from the definition could lead to an incorrect perception of the observed trends. Therefore, based on the definition from past studies[28], the trends for the widespread EREs (as shown in Supplementary Fig. 4) are also analyzed and are found to be in agreement with the observed trends. These add further to the proof of affirmation that the observed decline in the past two decades is not just an artifact or noise, but an actual trend albeit short-term.

The ISM months contribute to most of the mean and extreme precipitation in the CIR[45]. The frequency and intensity of these rains are tightly interrelated with the monsoonal circulations and moisture sources[46]. The convergence of moisture to the continent is key to the buoyancy of the moist air and intensification of the EREs has a significant year-to-year variation. Studies have suggested that the strong monsoon years get the majority of their moisture from the oceanic sources with the terrestrial sources having increased presence during the weak years[47]. The oceanic sources include the Arabian Sea, the Bay of Bengal, and

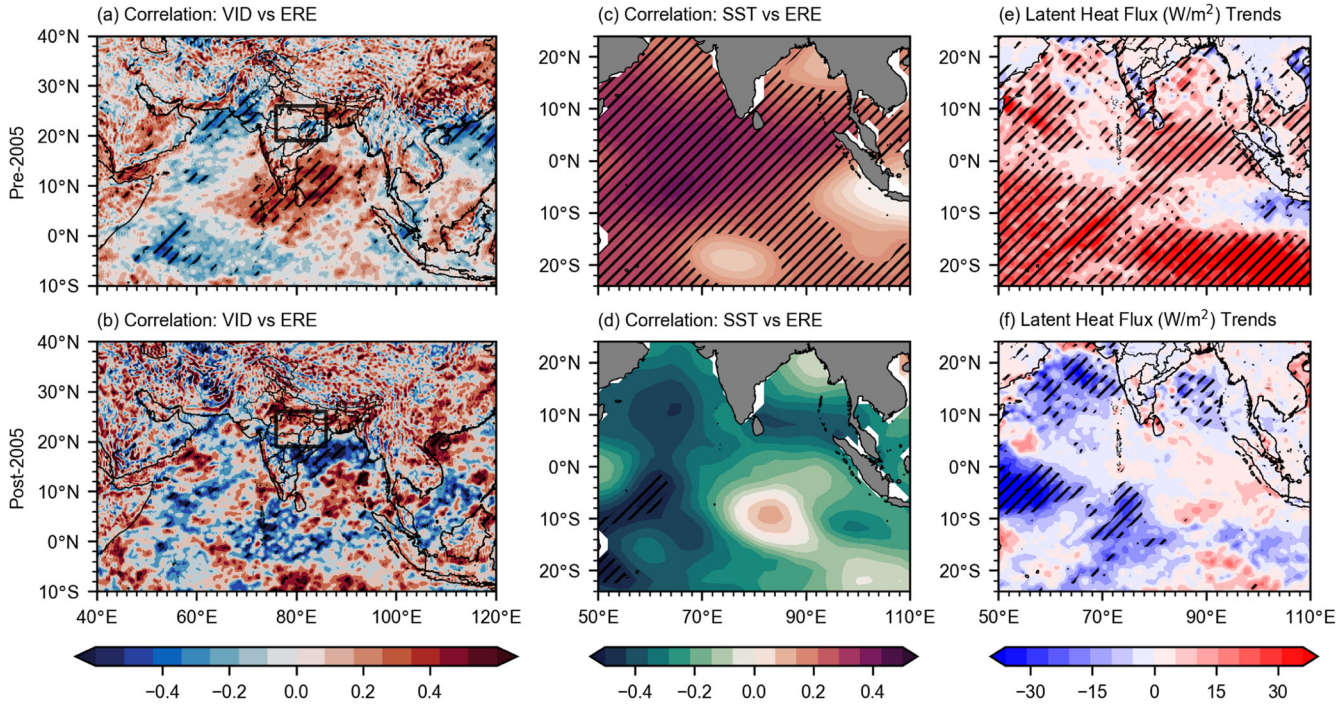

Fig. 2 Comparison of moisture dynamics between pre and post-2005. Correlation between the vertical integrated moisture transports (kg/ms) and the yearly ERE frequency (numbers) over CIR during JJAS in the period of **a** 1951–2005 and **b** 2005–2020. Correlation between the yearly ERE frequency over CIR (numbers) and sea surface temperature (°C) during JJAS for the period **c** 1901–2005, **d** 2005–2019. Trends of latent heat flux (W/m^2) during JJAS in the period **a** 1951–2005 and **b** 2005–2020. The hatching indicates the locations with more than 95% confidence levels. Dataset Utilized: IMD 0.25°, ERA5, ERSST.

the equatorial Indian Ocean, in the descending order of contribution[28]. While the Arabian Sea has had a steady presence of dominance throughout the years, the added contributions from the other remote oceanic sources make the strong monsoon years more active[46].

Past studies have suggested that the sea surface temperature modulation over the equatorial Indian Ocean [60°−90°E, 6°N–6°S] has a direct positive relationship with the CIR EREs, within the time period that was available for analysis at that time[23,48]. This region's SST regulates the evaporation and the atmospheric moisture content, which is proposed to feed the transport and convergence of moisture over CIR[23]. But including the recent year's data, this relationship is found to break down post-2005. Even with continually increasing sea surface temperature, the CIR ERE counts show a decreasing trend, as can be seen in Fig. 2. However, it is also observed from the same figure that the post-2005 evaporation over the entirety of the Indian Ocean basin shows declining trends, contradicting the pre-2005 period which is characterized by inclining evaporation. Thus, we have seen that the sea surface heating patterns do not agree with the recent ERE declines.

It is well-known that deep convection is essential in driving atmospheric circulation in the tropics. This mechanism initiates at the planetary boundary layer (PBL)[49], roughly encompassing the lower to mid-tropospheric columns. The upward flux of unstable air supplied from this zone is found to have direct correlations with the occurrence of deep convection[50]. More specifically, this updraft buoyancy strength is characterized by the moist static energy (MSE) profile of this part of the atmospheric column. MSE is a moist thermodynamic indicator of atmospheric stability[51], defined by the summation of the internal energy of an air parcel and its geopotential energy. An increased MSE decreases the stability of the atmosphere, making it conducive for moist convection[52].

On the Indian subcontinent, an increase in tropospheric MSE is often associated with the onset of ISM[53]. The atmospheric structures of MSE are known to vary from time to time, based on multiple factors. Recently, it is understood that the sub-cloud MSE is affected by absorbing aerosols like black carbons which are then found to perturb the low-level MSE profiles and gradients, driving the monsoonal deep convection centers northwards or northwestwards[54,55].

The vertical gradient of MSE in the PBL is the most significant criterion for identifying the potential for initiating convection. A vertically steeper MSE profile from the ground to the middle troposphere represents a more unstable atmosphere than a gradual MSE profile. As can be seen from Fig. 3, the vertically averaged MSE gradient shows a statistically significant decreasing trend (Supplementary Table 2) akin to the declining ERE trends. That is, the atmosphere, which was getting increasingly unstable since 1950, has begun to show signs of increasing stability post-2005. In the current case, the trends of the vertical gradient of MSE are consistent with trends of the EREs.

How do we expect the trends of the EREs and HREs to be related to the trends of seasonal mean rainfall, ISMR? It may be noted that the EREs and HREs come from small-scale convective events and contribute to about 7–10% of the seasonal total rainfall while that in LREs and MREs come from convective clusters and synoptic scale low-pressure systems (LPS) and contribute to >90% of seasonal rainfall[15]. Therefore, the trend of ISMR would be determined largely by the trends of LREs and MREs and hence trends of ISMR and those of LREs/MREs are expected to be the same. However, the trend of EREs/HREs is complementary to those of LREs/MREs. As a result, the trend of ISMR and those of EREs/HREs are expected to be opposite. As expected, the decreasing trend of ISMR over CI during 1950–2000 and the increasing trend after 2002 are exactly opposite to the trends of EREs during the same periods (Fig. 4a).

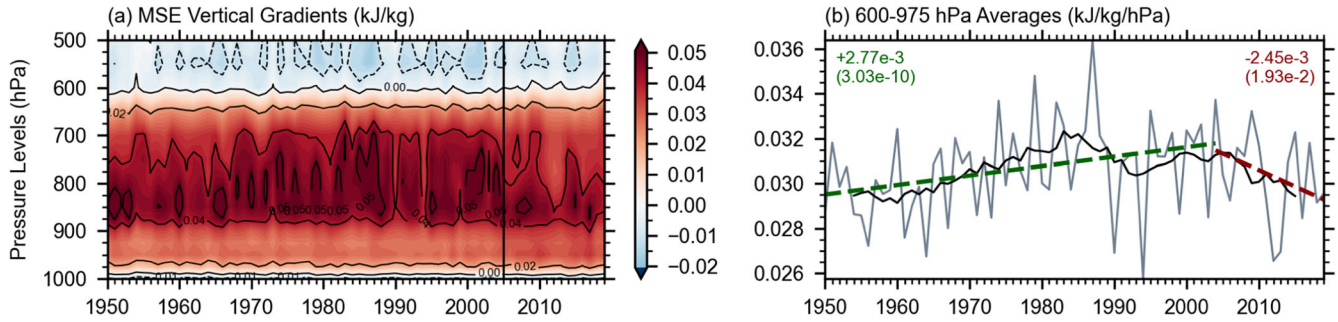

Fig. 3 Moist static energy trends. Contour time series of JJAS yearly averaged JJAS **a** vertical gradient of MSE (kJ/kg) over CIR. The black vertical line marks the year 2005. **b** Time series of 600–975 hPa averages of MSE gradient (kJ/kg/hPa) with the darker lines indicating 9-year running averages and the dashed lines indicating the linear trends during both periods. The trend value and the *p*-value (in brackets) of the corresponding trends are also shown. Dataset Utilized: IMD 0.25°.

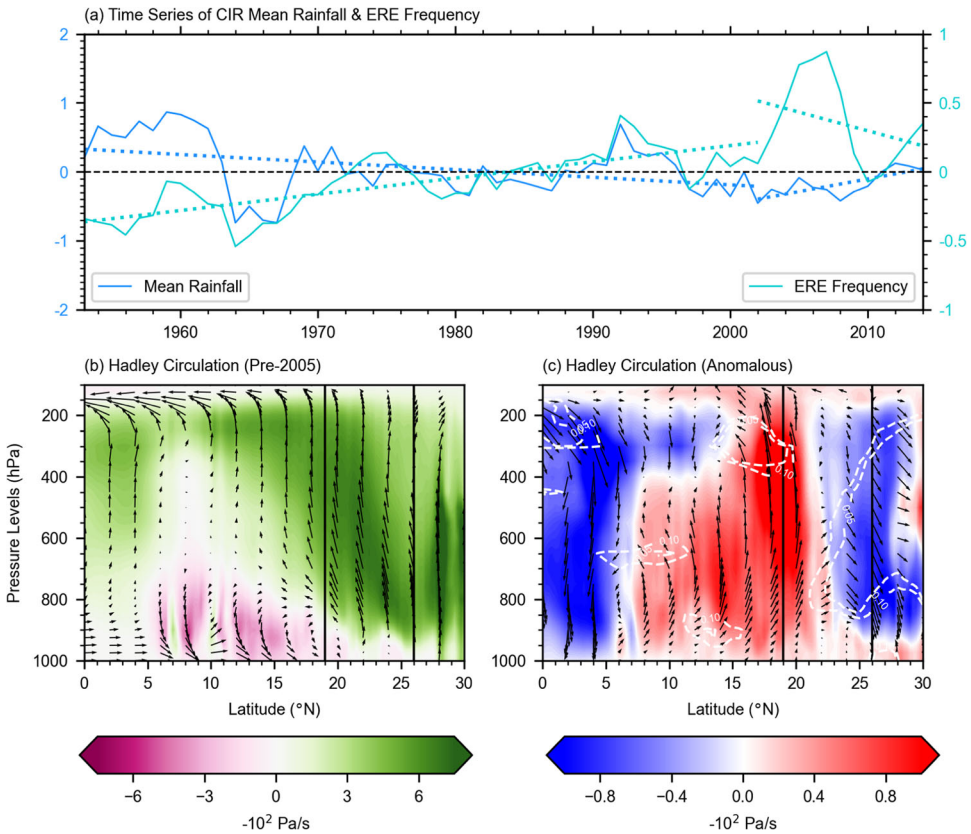

Fig. 4 Monsoon Hadley circulation trends. a Time series of five-year running means of the ISM precipitation anomalies (left axis; mm d^{-1}) and frequency (nos.) of ERE (right axis) over CIR during JJAS from 1953 to 2014 relative to the 1953–2014 base period. **b** ISM Hadley Circulation climatology, represented by the zonally averaged vertical velocity (−100 Pa/s) in the contours over 76-86°E. **c** Anomalous Hadley circulation cell during ISM, represented by the differences between pre-2005 and post-2005 of the zonal averages of vertical velocity (−100 Pa/s) in contours over 76–86°E. The white dashed lines are the contour lines of *p*-values of 0.05 and 0.1. The vertical lines mark the latitudes of CIR and the arrows represent both the vertical (−100 Pa/s) and meridional (m/s) velocities corresponding to the respective panels. Dataset Utilized: IMD 0.25°, ERA5.

Being a convectively coupled system, the seasonal mean rainfall (ISMR) is strongly correlated with the regional Hadley circulation associated with rising vertical motions along the regional Inter-Tropical Convergence Zone (ITCZ)[19]. Therefore, further explore the changes in the monsoonal Hadley circulation between the two periods, pre-2005 and post-2005. It can be seen from Fig. 4b during pre-2005 that the maximum vertical velocity of the monsoonal Hadley cell climatology lies between 10°N–23°N with orographic ascent beyond 25°N. However, the observation of the anomalous monsoonal Hadley Circulation between the two periods over CIR (Fig. 4c, Supplementary Fig. 6) between 10°N and 23°N indicates the presence of anomalous ascent during post-2005 compared to pre-2005. This is consistent with a decreasing trend of the monsoon Hadley (MH) circulation associated with a decreasing trend of ISMR and an increasing trend of the MH circulation associated with the increasing trend of ISMR (Fig. 4a). This agrees well with our observed ERE trends post-2005 and with the past hypothesis that the weakening MH circulation is accompanied by an increasing frequency of EREs/HREs while strengthening MH circulation is associated with a weakening frequency of EREs/HREs.

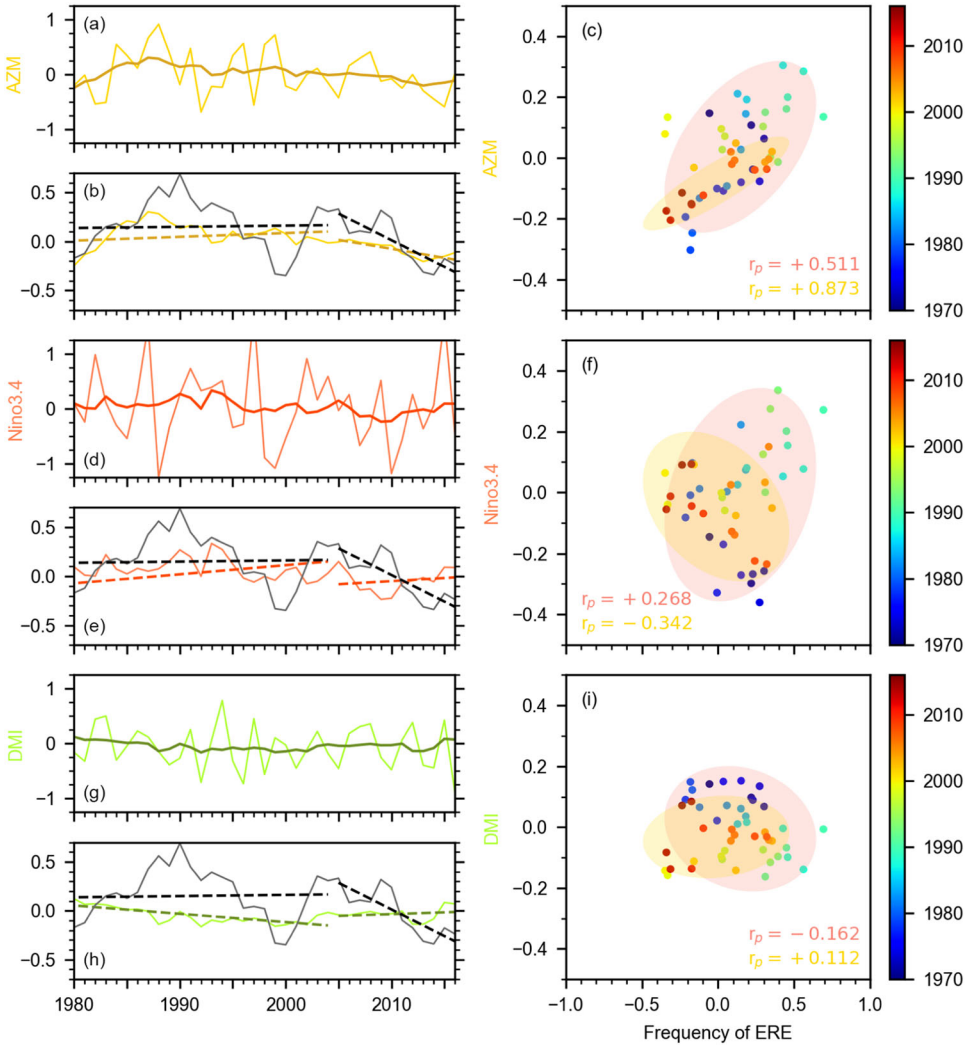

Fig. 5 Tropical climate drivers. Time Series of the yearly JJAS averaged detrended normalized indices of tropical climate drivers of **a** AZM, **d** Nino3.4, and **g** DMI, with the darker lines indicating the 9-year running averages. Time Series of 9-year running averages of the tropical drivers of **b** AZM, **e** Nino3.4, and **h** DMI, compared with the 9-year running average of CIR ISM ERE frequency, with the darker dashed lines indicating the pre-2005 and post-2005 linear trends. Scatter plots between the ERE frequency and the tropical climate drivers of **c** AZM, **f** Nino3.4, and **i** DMI, with the confidence ellipses representing the correlations during 1957-1968 (blue), 1968–2005 (salmon), and 2005–2016 (gold). Dataset Utilized: IMD 0.25°, ERA5, ERSST.

Apart from the regional moisture dynamics and local moist thermodynamics, the most important phenomena to factor in when understanding the temporal variation in the hydroclimate of a region are the various long-term climate drivers. The most important amongst numerous tropical climate drivers that affect the ISM include the El-Nino Southern Oscillation (ENSO/Nino3.4, Pacific Nino), the Atlantic Zonal Mode (AZM, Atlantic Nino), and the Indian Ocean Dipole (IOD/DMI, Indian Nino), driven by the Bjerknes feedback[56,57]. These drivers are often known to be the dominant modulators of precipitation in the ISM regions, often operating together but contradicting one another at times. ENSO and AZM possess a negative correlational relationship with the mean ISM rainfall[58–60], unlike the IOD which has a positive correlation. However, their relationships with precipitation extremes are complex. It has been suggested by previous studies that there is a strong correlation between the ISM rainfall extremes and ENSO, especially relevant when taken as a linear combination with the IOD[61]. For AZM, one study suggested a negative relationship with the ISM precipitation extremes[62].

From Fig. 5, on examination of the trends and correlations between these three tropical climate drivers and the ERE frequency trends in CIR, it can be observed that the AZM or the Atlantic Nino shows the best statistical significance with regard to both the rising and the declining phases upon the removal of intradecadal-scale variability. The Nino3.4 exhibits a weak positive correlation pre-2005 and a weak negative correlation post-2005 with the ERE frequency, both of which are not as statistically strong as AZM. The DMI exhibits even weaker statistical significance, showing a very weak negative correlation pre-2005 and a weak positive correlation post-2005. Although the exact reason for the observance of weak correlations for DMI and Nino 3.4 and strong correlations for AZM is elusive, this correlation analysis indicates that the AZM climate driver shows the best potential for being one of the causal reasons behind the observed ERE frequency decreasing trend observed post-2005. Past studies have produced many teleconnection mechanisms between the AZM and the ISM precipitation[63–65]. The most prominent of those include the eastward-moving equatorial Kelvin wave response[58,66] and the modulations in the upper tropospheric Asian jets[67] associated with anomalous Walker Circulation.

Apart from the above-mentioned primary factors and their potential impacts on the recent decline in CIR EREs, there are other

possible phenomena like the synoptic-scale activities that may have lent a hand towards the observed trends. It is well-known that Low-Pressure Systems (LPSs) are a significant contributor to the monsoonal precipitation extremes in CIR[68,69]. Studies have highlighted that decrease in low-pressure systems could cause decreases in ERE frequency in the North-Central Indian region during the recent decades. But the relationships largely remain uncertain[70] and it has been widely argued that the different components of LPS have differing impacts. The weaker LPS or the monsoonal lows are observed to have an in-phase relationship with the CIR ERE frequency since the 1950s whereas the stronger monsoonal depressions show an opposing relation[43]. This contrasting pattern is attributed mainly to various constraints caused by the atmosphere or the oceans in the background[71,72]. It has also been noted that the presence of LPSs alone is not sufficient to produce the large-scale EREs and that the secondary cyclonic vortices along with the LPSs are needed to create sufficient instability in the atmosphere for deep convection[73].

The second half of the 20th century has seen increasing numbers of LPSs propagating into the CIR, driven by the strengthened moisture transport across the equator[70], corresponding well with the observed increasing ERE frequency trends. However, in recent decades, studies have reported that the synoptic-scale disturbances have reduced and weakened significantly[74,75] in association with a poleward shift[69]. Such observations have largely been attributed to the response of ISM circulation and LPSs to the accelerated melting of the polar sea ice[74]. Besides these, other climate drivers like the Pacific Decadal Oscillations are also known to affect the monsoonal depressions[76] and thereby its associated rainfall into the CIR. These complex interactions between the LPSs and the CIR EREs deserve a future study of its own to explore in details its role in the recent ERE declines.

In this study, we have established that there is an ongoing declining trend in the number of extreme precipitation events over the central Indian region during the Indian summer monsoon season since 2005 that is robust across datasets and definitions. It is also noted that the observed short-term declining trend may be a part of a long-term 50–70-year multi-decadal oscillation.

We have also proposed that the observed trends are related to the changes in moisture sources and transport. The decreasing trend of MH circulation post-2005 is consistent with decreasing trends of EREs/HREs during the period. In addition, it is also noted that the correlation between the SST over the Equatorial Indian Ocean and the ERE frequency over CIR during the post-2005 period is insignificant and negative. This indicates that the recent decline is not due to regional SST changes but is driven by external drivers through the modulation of circulation and moist thermodynamic parameters.

Though the dynamics alone provide enough possible factors for reduction in ERE counts, understanding how that affects the local thermodynamics is also essential. Likewise, the local moist thermodynamics also support the observed trends. The surface gradient of MSE presents itself with switching trend signs post-2005, reducing in magnitude, indicating the increasing stability of the lower to middle troposphere, a region crucial for initiating deep convection.

We find a strong positive relationship between an important tropical climate driver namely the Atlantic Nino or the AZM and CIR ERE frequency during ISM. Thus, the AZM appears to be the 'external driver' that is responsible for modulating the local conditions and resulting in the ERE trend. This aspect of the study deserves a further detailed understanding of the exact teleconnection mechanism at multi-decadal timescales.

This study presents a compelling example of a decreasing trend during post-2005 that seems to be an exception to the norm of the expected increasing trend of extreme precipitation events in the backdrop of global warming and climate change. Our findings may have important implications for the increasing trend of hydrological disasters in India in the coming years. In response to decreasing frequency of EREs, can we expect the frequency and intensity of flash floods and landslides to decrease in the coming years? To address this question, we plan to examine the state-of-the-art CMIP6 climate models to test the reproducibility of these changes in the ERE trends and their impacts on the hydroclimate of the region. We hope that it would enhance our understanding and could aid in accurately predicting the trends of the monsoonal precipitation extremes to be able to help better with the socio-economic situations in the region.

METHODS

As mentioned in the Introduction, there are multiple ways of quantifying an extreme precipitation event. The absolute threshold approach is the major definition that was utilized throughout the analysis, with the other kinds used as verification for the robustness of the former. The absolute threshold employed in the study is 150 mm/day, in evidence from earlier studies. According to this definition, a rainfall event is considered an ERE when its precipitation goes past the specified threshold. So, for a particular spatial coordinate, the frequency of EREs in a year is characterized by how many days succeed the threshold value in rainfall. The frequency for the entire spatial region over a year is taken to be the sum of all the counts of every spatial coordinate for that year. In addition to the absolute threshold approach, the percentile threshold approach was also utilized, mainly to verify robustness across multiple definitions. In the latter, the only difference is, for a particular spatial grid point, the threshold was taken to be the n-th percentile of all years' daily precipitation. For the analysis, 99th, 99.5th, 99.9th, and 99.99th percentiles were used. These percentile thresholds are spatially varying unlike the former. The intensity of the EREs was calculated for a particular year, as the average of all ERE precipitation for a particular grid point, averaged over the required region.

For the other precipitation regimes, similar methods for the absolute threshold approach were followed. The LREs are categorized as the grid points with rainfall more than 0 but less than or equal to 5 mm/day, the MREs are categorized as the rainfall events greater than 5 mm/day but less than or equal to 100 mm/day, with the HREs having been defined as the grid points possessing rainfall more than 100 mm/day but less than or equal to 150 mm/day. The identification of the breakpoint of 2005 was done through the ruptures python library by employing the dynamic programming searching method with a linear model[77].

The vertically integrated moisture transport is calculated as the vertical integral of the product of wind speed (V) and the specific humidity (q) from 1000 to 300 hPa, illustrated in the following equation:

$$\mathrm{VIMT} = \frac{1}{g}\int_{P_{300}}^{P_{1000}} qV\mathrm{d}p \tag{1}$$

where g is the acceleration due to gravity and p is the pressure level.

The regional Hadley Circulation cell is computed by averaging the vertical velocity and the meridional winds for the Central India longitudes [19°N–26°N].

The moist static energy profiles are evaluated from the temperature and specific humidity profiles using the MetPy[78] library from Python. The formula used in the computation is as shown below:

$$\mathrm{MSE} = c_{\mathrm{pd}}T + gz + L_{\mathrm{v}}q \tag{2}$$

where c_{pd} denotes specific heat at constant pressure, T denotes absolute temperature, z denotes geopotential height and L_{v} denotes the latent heat of vaporization.

All of the figures in the study that portray linear trends show the least squares fit regressions calculated from SciPy library[79], with

the mentioned p-values having been obtained from the modified Mann–Kendall Test[80], computed from pymannkendall python library[81].

The Atlantic Zonal Mode was computed from the ERSST dataset, as the SST anomaly, averaged in the Atlantic Nino region [−20°E–10°E & −6°N–4°N]. As for the Nino3.4 and DMI, the data were obtained from the Physical Sciences Laboratory, National Oceanic and Atmospheric Administration (https://psl.noaa.gov/data/climateindices/list/).

DATA AVAILABILITY

All the data used in this study is publicly available and accessible. IMD data is available on the IMD portal at https://www.imdpune.gov.in/cmpg/Griddata/Rainfall_25_NetCDF.html. ECMWF fifth generation (ERA5) data can be accessed through https://www.ecmwf.int/en/forecasts/datasets/reanalysis-datasets/era5. TRMM-3B42, GPM-IMERG and ERSST data were downloaded directly from http://apdrc.soest.hawaii.edu/ using ERDDAP.

CODE AVAILABILITY

The source codes for the analysis of this study are available from the corresponding author upon reasonable request.

Received: 7 May 2022; Accepted: 10 August 2023;
Published online: 19 August 2023

REFERENCES

1. Falkenmark, M. Society's interaction with the water cycle: a conceptual framework for a more holistic approach. *Hydrol. Sci. J.* **42**, 451–466 (1997).
2. Utsumi, N., Seto, S., Kanae, S., Maeda, E. E. & Oki, T. Does higher surface temperature intensify extreme precipitation? *Geophys. Res. Lett.* **38**, L21704 (2011).
3. Muller, C. & Takayabu, Y. Response of precipitation extremes to warming: what have we learned from theory and idealized cloud-resolving simulations, and what remains to be learned? *Environ. Res. Lett.* **15**, 035001 (2020).
4. Roca, R. et al. On the water and energy cycles in the Tropics. *C. R. - Geosci.* **342**, 390–402 (2010).
5. Huang, P., Xie, S.-P., Hu, K., Huang, G. & Huang, R. Patterns of the seasonal response of tropical rainfall to global warming. *Nat. Geosci.* **6**, 357–361 (2013).
6. Xie, S.-P. et al. Global warming pattern formation: sea surface temperature and rainfall. *J. Clim.* **23**, 966–986 (2010).
7. Held, I. M. & Soden, B. J. Robust responses of the hydrological cycle to global warming. *J. Clim.* **19**, 5686–5699 (2006).
8. Seager, R., Naik, N. & Vecchi, G. A. Thermodynamic and dynamic mechanisms for large-scale changes in the hydrological cycle in response to global warming. *J. Clim.* **23**, 4651–4668 (2010).
9. Chou, C. et al. Increase in the range between wet and dry season precipitation. *Nat. Geosci.* **6**, 263–267 (2013).
10. Allen, M. R. & Ingram, W. J. Constraints on future changes in climate and the hydrologic cycle. *Nature* **419**, 228–232 (2002).
11. Mitchell, J. F., Wilson, C. & Cunnington, W. On CO2 climate sensitivity and model dependence of results. *Q. J. R. Meteorol.* **113**, 293–322 (1987).
12. Wentz, F. J., Ricciardulli, L., Hilburn, K. & Mears, C. How much more rain will global warming bring? *Science* **317**, 233–235 (2007).
13. Bollasina, M. A., Ming, Y. & Ramaswamy, V. Anthropogenic aerosols and the weakening of the South Asian summer monsoon. *Science* **334**, 502–505 (2011).
14. Roxy, M. & Chaithra, S. *Impacts of Climate Change on the Indian Summer Monsoon* (Ministry of Environment, Forest and Climate Change (MoEF&CC), Government of …, 2018).
15. Goswami, B. N., Venugopal, V., Sengupta, D., Madhusoodanan, M. & Xavier, P. K. Increasing trend of extreme rain events over India in a warming environment. *Science* **314**, 1442–1445 (2006).
16. Sinha, A. et al. Trends and oscillations in the Indian summer monsoon rainfall over the last two millennia. *Nat. Commun.* **6**, 6309 (2015).
17. Rajesh, P., Goswami, B., Choudhury, B. & Zahan, Y. Large sensitivity of simulated Indian summer monsoon rainfall (ISMR) to global warming: implications of ISMR projections. *J. Geophys. Res. Atmos.* **126**, e2020JD033511 (2021).
18. Jin, Q. & Wang, C. A revival of Indian summer monsoon rainfall since 2002. *Nat. Clim. Change* **7**, 587–594 (2017).
19. Goswami, B. N., Krishnamurthy, V. & Annmalai, H. A broad-scale circulation index for the interannual variability of the Indian summer monsoon. *Q. J. R. Meteorol.* **125**, 611–633 (1999).
20. Webster, P. J. & Yang, S. Monsoon and ENSO: selectively interactive systems. *Q. J. R. Meteorol.* **118**, 877–926 (1992).
21. Zahan, Y., Mahanta, R., Rajesh, P. & Goswami, B. Impact of climate change on North-East India (NEI) summer monsoon rainfall. *Clim. Change* **164**, 1–19 (2021).
22. Zahan, Y., Rajesh, P., Choudhury, B. A. & Goswami, B. Why Indian summer monsoon circulation indices? Fidelity in representing rainfall variability and teleconnections. *Q. J. R. Meteorol.* **147**, 1300–1316 (2021).
23. Rajeevan, M., Bhate, J. & Jaswal, A. K. Analysis of variability and trends of extreme rainfall events over India using 104 years of gridded daily rainfall data. *Geophys. Res. Lett.* **35**, L18707 (2008).
24. Falga, R. & Wang, C. The rise of Indian summer monsoon precipitation extremes and its correlation with long-term changes of climate and anthropogenic factors. *Sci. Rep.* **12**, 1–11 (2022).
25. Kumari, A., Kumar, P., Dubey, A. K., Mishra, A. K. & Saharwardi, M. S. Dynamical and thermodynamical aspects of precipitation events over India. *Int. J. Climatol.* **42**(5), 3094–3106 (2021).
26. Papalexiou, S. M. & Montanari, A. Global and regional increase of precipitation extremes under global warming. *Water Resour. Res.* **55**, 4901–4914 (2019).
27. Easterling, D. R. et al. Observed climate variability and change of relevance to the biosphere. *J. Geophys. Res. Atmos.* **105**, 20101–20114 (2000).
28. Roxy, M. K. et al. A threefold rise in widespread extreme rain events over central India. *Nat. Commun.* **8**, 1–11 (2017).
29. Karl, T. R. & Knight, R. W. Secular trends of precipitation amount, frequency, and intensity in the United States. *Bull. Am. Meteorol. Soc.* **79**, 231–242 (1998).
30. Trenberth, K. E., Dai, A., Rasmussen, R. M. & Parsons, D. B. The changing character of precipitation. *Bull. Am. Meteorol. Soc.* **84**, 1205–1218 (2003).
31. Kumari, A. & Kumar, P. Contrasting changes in precipitation events during active and break spells of Indian summer monsoon in recent decades. *Clim. Dyn* **59**, 887–902 (2022).
32. Rajeevan, M. & Nayak, S. *Observed Climate Variability and Change over the Indian Region* (Springer, 2017).
33. Goswami, B. B., Mukhopadhyay, P., Mahanta, R. & Goswami, B. Multiscale interaction with topography and extreme rainfall events in the northeast Indian region. *J. Geophys. Res. Atmos.* **115**, D12114 (2010).
34. Pai, D., Sridhar, L., Badwaik, M. & Rajeevan, M. Analysis of the daily rainfall events over India using a new long period (1901–2010) high resolution (0.25 × 0.25) gridded rainfall data set. *Clim. Dyn.* **45**, 755–776 (2015).
35. Singh, D. Implications of a varying observational network for accurately estimating recent climate trends. *Geophys. Res. Lett.* **46**, 5430–5435 (2019).
36. Huffman, G. J. et al. The TRMM multisatellite precipitation analysis (TMPA): quasi-global, multiyear, combined-sensor precipitation estimates at fine scales. *J. Hydrometeorol.* **8**, 38–55 (2007).
37. Huffman, G. J. et al. NASA global precipitation measurement (GPM) integrated multi-satellite retrievals for GPM (IMERG). *Algorithm Theor. Basis Doc. Version* **4**, 26 (2015).
38. Hersbach, H. et al. ERA5 hourly data on single levels from 1979 to present. *Copernicus Climate Change Service (C3S) Climate Data Store (CDS)* **10**, (2018).
39. Hersbach, H. et al. The ERA5 global reanalysis. *Q. J. R. Meteorol.* **146**, 1999–2049 (2020).
40. Huang, B. et al. Extended reconstructed sea surface temperature, version 5 (ERSSTv5): upgrades, validations, and intercomparisons. *J. Clim.* **30**, 8179–8205 (2017).
41. Adve, N. *India in a Warming World* 64–78 (Oxford University Press, 2019).
42. Maharana, P., Agnihotri, R. & Dimri, A. Changing Indian monsoon rainfall patterns under the recent warming period 2001–2018. *Clim. Dyn.* **57**, 2581–2593 (2021).
43. Krishnan, R. et al. *Assessment of Climate Change Over the Indian Region: a Report of the Ministry of Earth Sciences (MOES), Government of India* (Springer Nature, 2020).
44. Pendergrass, A. G. What precipitation is extreme? *Science* **360**, 1072–1073 (2018).
45. Suthinkumar, P., Babu, C. & Varikoden, H. Spatial distribution of extreme rainfall events during 2017 southwest monsoon over Indian subcontinent. *Pure Appl. Geophys.* **176**, 5431–5443 (2019).
46. Kathayat, G. et al. Interannual oxygen isotope variability in Indian summer monsoon precipitation reflects changes in moisture sources. *Commun. Earth Environ.* **2**, 1–10 (2021).
47. Pathak, A., Ghosh, S., Kumar, P. & Murtugudde, R. Role of oceanic and terrestrial atmospheric moisture sources in intraseasonal variability of Indian summer monsoon rainfall. *Sci. Rep.* **7**, 1–11 (2017).
48. Krishnan, R. et al. Deciphering the desiccation trend of the South Asian monsoon hydroclimate in a warming world. *Clim. Dyn.* **47**, 1007–1027 (2016).
49. de Szoeke, S. P. Variations of the moist static energy budget of the tropical Indian Ocean atmospheric boundary layer. *J. Atmos. Sci.* **75**, 1545–1551 (2018).

50. Raymond, D. J. Regulation of moist convection over the west Pacific warm pool. *J. Atmos. Sci.* **52**, 3945–3959 (1995).
51. Yano, J. I. & Ambaum, M. H. Moist static energy: definition, reference constants, a conservation law and effects on buoyancy. *Q. J. R. Meteorol.* **143**, 2727–2734 (2017).
52. Neelin, J. D. & Zeng, N. A quasi-equilibrium tropical circulation model—formulation. *J. Atmos. Sci.* **57**, 1741–1766 (2000).
53. Chakraborty, A. & Agrawal, S. Role of West Asian surface pressure in summer monsoon onset over central India. *Environ. Res. Lett.* **12**, 074002 (2017).
54. Wang, C., Kim, D., Ekman, A. M., Barth, M. C. & Rasch, P. J. Impact of anthropogenic aerosols on Indian summer monsoon. *Geophys. Res. Lett.* **36**, L21704 (2009).
55. Jin, Q., Wei, J., Lau, W. K., Pu, B. & Wang, C. Interactions of Asian mineral dust with Indian summer monsoon: Recent advances and challenges. *Earth-Sci. Rev.* **215**, 103562 (2021).
56. Wang, C., Deser, C., Yu, J.-Y., DiNezio, P. & Clement, A. El Niño and southern oscillation (ENSO): a review. In *Coral Reefs of the Eastern Tropical Pacific*, 85–106 (Springer, 2017).
57. Lübbecke, J. F. & McPhaden, M. J. Symmetry of the Atlantic Niño mode. *Geophys. Res. Lett.* **44**, 965–973 (2017).
58. Sabeerali, C., Ajayamohan, R., Bangalath, H. K. & Chen, N. Atlantic zonal mode: an emerging source of Indian summer monsoon variability in a warming world. *Geophys. Res. Lett.* **46**, 4460–4467 (2019).
59. Mooley, D. & Parthasarathy, B. Indian summer monsoon and El Nino. *Pure Appl. Geophys.* **121**, 339–352 (1983).
60. Rasmusson, E. M. & Carpenter, T. H. The relationship between eastern equatorial Pacific sea surface temperatures and rainfall over India and Sri Lanka. *Mon. Weather Rev.* **111**, 517–528 (1983).
61. Gadgil, S., Vinayachandran, P., Francis, P. & Gadgil, S. Extremes of the Indian summer monsoon rainfall, ENSO and equatorial Indian Ocean oscillation. *Geophys. Res. Lett.* **31**, L12213 (2004).
62. Jamshadali, V., Reji, M., Varikoden, H. & Vishnu, R. Spatial variability of South Asian summer monsoon extreme rainfall events and their association with global climate indices. *J. Atmos. Sol.-Terr. Phys.* **221**, 105708 (2021).
63. Yadav, R. K., Srinivas, G. & Chowdary, J. S. Atlantic Niño modulation of the Indian summer monsoon through Asian jet. *NPJ Clim. Atmos. Sci.* **1**, 23 (2018).
64. Kucharski, F., Bracco, A., Yoo, J. & Molteni, F. Atlantic forced component of the Indian monsoon interannual variability. *Geophys. Res. Lett.* **35**, L04706 (2008).
65. Kucharski, F., Bracco, A., Yoo, J. & Molteni, F. Low-frequency variability of the Indian monsoon–ENSO relationship and the tropical Atlantic: the "weakening" of the 1980s and 1990s. *J. Clim.* **20**, 4255–4266 (2007).
66. Pottapinjara, V. et al. Simulation of interannual relationship between the Atlantic zonal mode and Indian summer monsoon in CFSv2. *Clim. Dyn.* **57**, 353–373 (2021).
67. Yadav, R. K., Srinivas, G. & Chowdary, J. S. Atlantic Niño modulation of the Indian summer monsoon through Asian jet. *NPJ Clim. Atmos. Sci.* **1**, 1–11 (2018).
68. Sinha, A., Gupta, M., Srujan, K. S., Kodamana, H. & Sandeep, S. Prediction of synoptic-scale sea level pressure over the Indian monsoon region using deep learning. *IEEE Geosci. Remote Sens.* **19**, 1–5 (2021).
69. Sandeep, S., Ajayamohan, R., Boos, W. R., Sabin, T. & Praveen, V. Decline and poleward shift in Indian summer monsoon synoptic activity in a warming climate. *Proc. Natl Acad. Sci. USA* **115**, 2681–2686 (2018).
70. You, Y. & Ting, M. Observed trends in the South Asian monsoon low-pressure systems and rainfall extremes since the late 1970s. *Geophys. Res. Lett.* **48**, e2021GL092378 (2021).
71. Prajeesh, A., Ashok, K. & Rao, D. B. Falling monsoon depression frequency: A Gray-Sikka conditions perspective. *Sci. Rep.* **3**, 2989 (2013).
72. Rao, B. S., Rao, D. B. & Rao, V. B. Decreasing trend in the strength of Tropical Easterly Jet during the Asian summer monsoon season and the number of tropical cyclonic systems over Bay of Bengal. *Geophys. Res. Lett.* **31**, L14103 (2004).
73. Nikumbh, A. C., Chakraborty, A., Bhat, G. & Frierson, D. M. Large-scale extreme rainfall-producing synoptic systems of the Indian summer monsoon. *Geophys. Res. Lett.* **47**, e2020GL088403 (2020).
74. Chandra, V., Sandeep, S., Suhas, E. & Subramanian, A. C. Weakening of Indian Summer Monsoon synoptic activity in response to Polar Sea Ice Melt induced by albedo reduction in a climate model. *Earth Space Sci.* **9**, e2021EA002185 (2022).
75. Prathipati, V. K., CV, N. & Konatham, P. Inconsistency in the frequency of rainfall events in the Indian summer monsoon season. *Int. J. Climatol.* **39**, 4907–4923 (2019).
76. Vishnu, S., Francis, P. A., Shenoi, S. C. & Ramakrishna, S. S. V. S. On the relationship between the Pacific Decadal Oscillation and monsoon depressions over the Bay of Bengal. *Atmos. Sci. Lett.* **19**, e825 (2018).
77. Truong, C., Oudre, L. & Vayatis, N. Selective review of offline change point detection methods. *Signal Process.* **167**, 107299 (2020).
78. May, R. M. et al. MetPy: a Python package for meteorological data. Version 0.12 2, Unidata, https://doi.org/10.5065/D6WW7G29 (2020). Accessed 28 June 2021. Available online at: https://github.com/Unidata/MetPy.
79. Virtanen, P. et al. SciPy 1.0: fundamental algorithms for scientific computing in Python. *Nat. Methods* **17**, 261–272 (2020).
80. Yue, S. & Wang, C. The Mann–Kendall test modified by effective sample size to detect trend in serially correlated hydrological series. *Water Resour. Manag.* **18**, 201–218 (2004).
81. Hussain, M. & Mahmud, I. pyMannKendall: a python package for non parametric Mann Kendall family of trend tests. *J. Open Source Softw.* **4**, 1556 (2019).

ACKNOWLEDGEMENTS

This research work was supported by the Indian Institute of Science Education and Research Mohali, Government of India. BNG thanks the Science and Engineering Research Board (SERB), Government of India for a Fellowship and Research Grant. We thank ISRO's Disaster Management Support Program (DMSP) at IIRS, for funding under IIRS/DO/DMSP-ASCB/AS/2022/08. The authors acknowledge and appreciate the anonymous reviewers for their constructive feedback, which helped in improving the quality of our work.

AUTHOR CONTRIBUTIONS

R.A. and C.B. conceptualized the problem, conducted the analysis related to the study, and wrote the original manuscript. B.N.G. contributed towards editing, reviewing, revising, and finalizing the manuscript. All the co-authors contributed to the discussion of results and the final version of the manuscript.

COMPETING INTERESTS

The authors declare no competing interests.

ADDITIONAL INFORMATION

Supplementary information The online version contains supplementary material available at https://doi.org/10.1038/s41612-023-00450-y.

Correspondence and requests for materials should be addressed to Raju Attada.

Reprints and permission information is available at http://www.nature.com/reprints

Publisher's note Springer Nature remains neutral with regard to jurisdictional claims in published maps and institutional affiliations.